IEEE Access
Multidisciplinary ⋮ Rapid Review ⋮ Open Access Journal

Received September 13, 2021, accepted September 18, 2021, date of publication September 24, 2021,
date of current version October 5, 2021.

Digital Object Identifier 10.1109/ACCESS.2021.3115563

Quasi-Coherent Phase-Based Localization and Tracking of Incoherently Transmitting Radio Beacons

ERIK SIPPEL[1], MARKUS HEHN[1], (Graduate Student Member, IEEE), TOBIAS KOEGEL[1], PATRICK GRÖSCHEL[1], (Member, IEEE), ANDREAS HOFMANN[1], STEFAN BRÜCKNER[1], JOHANNA GEISS[1], (Graduate Student Member, IEEE), ROBERT SCHOBER[2], AND MARTIN VOSSIEK[1], (Fellow, IEEE)

[1]Institute of Microwaves and Photonics, Friedrich–Alexander University Erlangen–Nürnberg, 91058 Erlangen, Germany
[2]Institute for Digital Communications, Friedrich–Alexander University Erlangen–Nürnberg, 91058 Erlangen, Germany

Corresponding author: Erik Sippel (erik.sippel@fau.de)

This work was supported by the Deutsche Forschungsgemeinschaft (DFG, German Research Foundation) under Grant SFB 1483–Project-ID 44241933.

ABSTRACT The direct measurement of distance-dependent information between wireless units represents a challenge for wireless locating systems, because it requires the exact time synchronization of separate wireless units. To avoid these synchronization efforts, many wireless locating systems only evaluate phase difference of arrival (PDOA) measurements. While simple PDOA localization techniques rely on multilateration, advanced PDOA concepts like the holographic extended Kalman filter (HEKF) directly evaluate the measured phases without non-linear preprocessing. However, these differential phase measurement approaches are less sensitive than systems that can measure absolute phase variations, which allow the tracking of much smaller position changes than the signal's carrier wavelength. This paper proposes to extend the HEKF by the evaluation of absolute phases in an incoherent measurement setup, which consists of a continuous wave (CW) beacon and several receivers. The developed quasi-coherent holographic extended Kalman filter (QCHEKF) uses the overdetermined PDOA measurements to estimate the phase–frequency relation between each beacon–receiver pair. Then, the established phase–frequency relations allow the evaluation of absolute phase measurements and, thus, the accurate localization and tracking of a simple, unsynchronized, narrowband CW beacon, even under severe multipath conditions. This novel concept is experimentally validated via 3D localization results in a challenging indoor scenario using a 24 GHz CW measurement setup. Here, the QCHEKF improves the achieved localization accuracy in comparison to the HEKF by 35 % from 0.78 cm to 0.51 cm, while the maximum deviation from the trajectory reduces by 68 % from 5 cm to 1.6 cm. Furthermore, the QCHEKF enables the exact tracking of fast changes in direction, which is usually a significant challenge for standard wireless target tracking systems.

INDEX TERMS Radar, Kalman filters, incoherent measurements, localization, array signal processing.

I. INTRODUCTION

Nowadays, positioning systems are used for many applications, such as logistics, automation, and autonomous driving [1]. In the literature, many measurement concepts have been proposed for localization, such as optical systems [2], ultrasonic systems [3], systems based on electric or magnetic field strengths [4], as well as electromagnetic waves [1]. Since communication devices, which emit and receive electromagnetic waves, are widely spread these days, wave-based localization is a common method of choice [5].

Electromagnetic waves can be used in different ways to gain information about a target's position. Evaluating the received signal strength (RSS) [6] to localize a target is challenging due to strong RSS variability with the measurement conditions [7]. However, neural networks can be used to learn an environment-dependent signal map [8], [9] and enable reliable indoor localization despite the RSS variability, particularly in combination with Kalman filtering [10]. Measuring the time of arrival (TOA) yields more reliable

The associate editor coordinating the review of this manuscript and approving it for publication was Di He.

This work is licensed under a Creative Commons Attribution 4.0 License. For more information, see https://creativecommons.org/licenses/by/4.0/

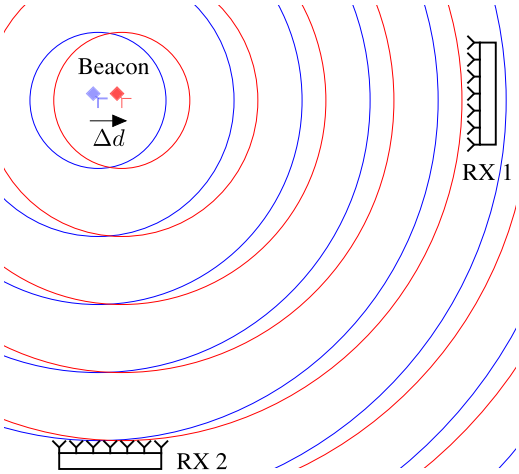

FIGURE 1. Measurement setup with two receiver arrays and one beacon, which moves the distance Δd and emits spherical waves.

distance information by evaluating the time-dependent phase relation for different frequencies within a limited bandwidth [1]. Unfortunately, available bandwidth is often limited due to governmental restrictions and implementation issues [11]. Hence, a tremendous effort is necessary to enable highly accurate ultra wide band (UWB) positioning [12]–[16], thereby providing localization results with errors of less than 1 cm.

Instead of evaluating the phases for different frequencies, phase difference of arrival (PDOA) systems evaluate the phase relation between spatially distributed antennas [11], as illustrated in Fig. 1. The most popular processing method is to estimate the angle of arrival (AOA) [17] for each beacon–receiver (RX) pair. Then, the AOA information at different RXs is combined to localize the beacon [18]–[20]. Since the phase-based AOA estimation results in undesired noise shaping, the accuracy of any successive signal processing is degraded [21] and, hence, a direct evaluation of phases is desirable. Therefore, holographic localization was proposed, which matches the received phases with hypothetical beacon positions using computational expensive brute force searches, as in [22]. To reduce the computational effort and further increase localization accuracy, the holographic extended Kalman filter (HEKF) was proposed in [23], which recursively estimates a beacon's position by evaluating the phase differences, measured between every antenna pair of each RX array.

PDOA systems inherently assume incoherent measurement principles, allowing localization with arbitrarily modulated signals based on relative phases [23]. However, evaluating absolute phases, which are related to TOA measurements between wireless units, provides a much higher sensitivity to position changes. Therefore, radio frequency identification (RFID) systems are often implemented with coherent beacons, as in [22]. Here, implementing coherent beacons depicts a challenging task, which can be solved by switched injection locking [24]. The relative phase information between measurements can then be used to improve localization accuracy, as in [25]. Most often, the time-dependent phase relation is used to estimate velocities based on the Doppler frequency [26]. The Doppler information can then be well fused with AOA estimations [27], [28]. However, the Doppler frequency estimation implicitly assumes a constant velocity for the evaluated time frame, which is not sufficiently valid for an accelerating beacon in a highly accurate indoor positioning system. In this work, the phases will be evaluated directly.

To combine the advantages of incoherent radio frequency beacons, which are easy to implement, and the high sensitivity of coherent measurements, we propose a novel concept to localize an incoherent continuous wave (CW) beacon. In Fig. 1, the HEKF's phase difference evaluation between the different antennas of RX 1 enables absolute positioning of the CW beacon in the vertical direction, while RX 2 provides absolute position information in the horizontal direction. However, since the time-dependent phase relation of CW beacons is deterministic, except for phase noise and frequency instability [29], [30], beacon movements toward a receiving antenna can be effectively detected by its absolute phase measurements. In Fig. 1, the small position change Δd of the beacon in the horizontal direction can be accurately detected via the absolute phase measurements at RX 1, while the absolute phase measurements at RX 2 remain nearly constant.

The HEKF presented in [23] consists of a constant velocity system state model and the evaluation of phase differences in the state update. The QCHEKF extends the HEKF by the evaluation of absolute phase measurements to take advantage of their high measurement sensitivity. To involve the time-dependency of the absolute phase measurements in the incoherent CW measurement setup, the QCHEKF extends the HEKF's constant velocity model via a constant frequency model for each beacon–receiver pair. To estimate this phase–frequency relation between each beacon–RX pair, the QCHEKF inherently uses the absolute position information gathered from the phase differences. Afterwards, the constant frequency model provides absolute phase measurement estimations, which are used via the quasi-coherent phase evaluation to improve the localization in comparison to the pure phase difference-based HEKF. Due to the direct evaluation of phases, the QCHEKF completely omits hindering preprocessing steps, such as the AOA or the Doppler frequency estimation. This novel concept is validated by 3D indoor localization results using a 24 GHz measurement setup with strong multipath propagation. For the presented trajectory, the QCHEKF localization result yields a 2D root mean squared error of 0.51 cm and a 2D maximum error of 1.6 cm and, hence, is comparable to the best UWB localization results, despite the usage of a narrow band measurement setup. The QCHEKF is able to detect rapid changes of direction, which is a standard problem in target tracking [31].

The remainder of this paper is organized as follows. In Section II, the system model is presented, and the novel QCHEKF is introduced in Section III. In Section IV, the

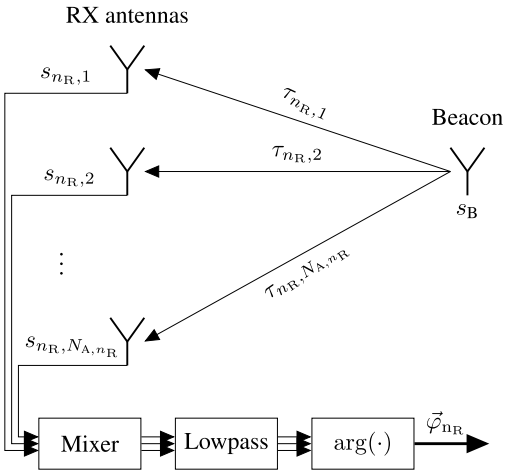

FIGURE 2. Illustration of the measurement model for one antenna array, receiving the signal of one beacon.

algorithm is validated via measurements. Finally, the article is finishes with a conclusion.

Notation: In this paper, $\vec{(\cdot)}$ represents a vector, matrices are denoted in bold letters, arg(·) evaluates the phase of a complex number and $|\cdot|$ is the absolute value. The transposition of a vector is calculated by $(\cdot)^{\mathrm{T}}$. A normally distributed vector with mean $\vec{\mu}$ and covariance matrix $\boldsymbol{C}$ is denoted as $\mathcal{N}(\vec{\mu}, \boldsymbol{C})$. $\|\cdot\|_2$ denotes the Euclidean norm. In the following, all phases will be mapped to $(-\pi, \pi]$ using

$$\mathrm{mod}'_{2\pi}(\cdot) = \begin{cases} \mathrm{mod}_{2\pi}(\cdot) & \text{if } \mathrm{mod}_{2\pi}(\cdot) \leq \pi \\ \mathrm{mod}_{2\pi}(\cdot) - 2\pi & \text{if } \mathrm{mod}_{2\pi}(\cdot) > \pi. \end{cases} \tag{1}$$

II. MODEL DESCRIPTION

In this section, the system model is described. First, the signal model chain from the beacon to one RX array, as illustrated in Fig. 2, is presented. Then, the measurement noise model is discussed. Finally, the system model describing the movement and oscillator behavior is presented.

A. SIGNAL MODEL

A moving beacon, located at time t at $\vec{p}_{\mathrm{B}}(t) = [x_{\mathrm{B}}(t), y_{\mathrm{B}}(t), z_{\mathrm{B}}(t)]^{\mathrm{T}}$, emits the signal

$$s_{\mathrm{B}}(t) = A_{\mathrm{B}} \cos(2\pi f_{\mathrm{B}} t + \phi_{\mathrm{B}}(t)), \tag{2}$$

where A_{B} denotes the signal's unknown amplitude, f_{B} denotes the approximate known transmit frequency, and $\phi_{\mathrm{B}}(t)$ denotes the transmit phase, which models both slowly varying frequency deviation and phase noise [29]. The signal is received by N_{R} receive antenna arrays, with the n_{R}th array comprising $N_{\mathrm{A},n_{\mathrm{R}}}$ antennas. The receive signal at the n_{A}th antenna of the n_{R}th array, located at $\vec{p}_{n_{\mathrm{R}},n_{\mathrm{A}}} = [x_{n_{\mathrm{R}},n_{\mathrm{A}}}, y_{n_{\mathrm{R}},n_{\mathrm{A}}}, z_{n_{\mathrm{R}},n_{\mathrm{A}}}]^{\mathrm{T}}$, is given by

$$s_{n_{\mathrm{R}},n_{\mathrm{A}}}(t) = A_{\mathrm{B}} a_{n_{\mathrm{R}},n_{\mathrm{A}}} \cos(2\pi f_{\mathrm{B}}(t - \tau_{n_{\mathrm{R}},n_{\mathrm{A}}}(t)) + \phi_{\mathrm{B}}(t)), \tag{3}$$

where $a_{n_{\mathrm{R}},n_{\mathrm{A}}}$ denotes the unknown signal attenuation caused by path loss, the receive and transmit antenna characteristics, and amplification factors in the processing chain, and

$$\tau_{n_{\mathrm{R}},n_{\mathrm{A}}}(t) = \frac{\|\vec{p}_{\mathrm{B}}(t) - \vec{p}_{n_{\mathrm{R}},n_{\mathrm{A}}}\|_2}{c_0} \tag{4}$$

denotes the signal's propagation time from the beacon to the antenna, with c_0 denoting the speed of light. At the n_{R}th antenna array, the signal is first mixed using a CW signal with frequency $f_{n_{\mathrm{R}}}$ and time varying phase $\phi_{n_{\mathrm{R}}}(t)$, which is also corrupted by phase noise, and then low-pass filtered, yielding the baseband signal

$$\begin{aligned} & s_{\mathrm{BB},n_{\mathrm{R}},n_{\mathrm{A}}}(t) \\ &= \mathrm{LP}\left(\mathrm{e}^{-\mathrm{j}(2\pi f_{n_{\mathrm{R}}} t + \phi_{n_{\mathrm{R}}}(t))} \cdot s_{n_{\mathrm{R}},n_{\mathrm{A}}}(t)\right) \\ &= A_{\mathrm{B}} a_{n_{\mathrm{R}},n_{\mathrm{A}}} \mathrm{e}^{\mathrm{j}\left(2\pi (f_{\mathrm{B}} - f_{n_{\mathrm{R}}})t - 2\pi f_{\mathrm{B}} \tau_{n_{\mathrm{R}},n_{\mathrm{A}}}(t) + \phi_{\mathrm{B}}(t) - \phi_{n_{\mathrm{R}}}(t)\right)} \\ &= A_{\mathrm{B}} a_{n_{\mathrm{R}},n_{\mathrm{A}}} \mathrm{e}^{\mathrm{j}\left(2\pi \Delta f'_{n_{\mathrm{R}}} t - 2\pi f_{\mathrm{B}} \tau_{n_{\mathrm{R}},n_{\mathrm{A}}}(t) + \Delta\phi'_{n_{\mathrm{R}}}(t)\right)} \end{aligned} \tag{5}$$

where $\Delta f'_{n_{\mathrm{R}}} = f_{\mathrm{B}} - f_{n_{\mathrm{R}}}$ denotes the frequency difference and $\Delta\phi'_{n_{\mathrm{R}}}(t) = \phi_{\mathrm{B}}(t) - \phi_{n_{\mathrm{R}}}(t)$ denotes the time varying unknown phase difference between the RX and the beacon, which is corrupted by their combined phase noise. Assuming the frequency difference $\Delta f'_{n_{\mathrm{R}}}$ is small enough to satisfy $\Delta f'_{n_{\mathrm{R}}} \ll \frac{1}{2T_{\mathrm{S}}}$, with T_{S} denoting the time between two sampling instances, the sampling theorem is satisfied and, therefore, the complete setup can be described solely at the discrete time instances $t = kT_{\mathrm{S}}$. From now on, for every variable, the time step information is marked in the index as $\mathrm{variable}_k = \mathrm{variable}(kT_{\mathrm{S}})$.

To separate the influence of the measurement system's frequency and phase relations from the influence of the beacon's movement on the measured phases, the beacon–RX phase difference $\Delta\phi_{n_{\mathrm{R}},k}$ in (5) at time step k is defined as

$$\Delta\phi_{n_{\mathrm{R}},k} = 2\pi \Delta f'_{n_{\mathrm{R}}} k T_{\mathrm{S}} + \Delta\phi'_{n_{\mathrm{R}},k}. \tag{6}$$

Expressing the slowly varying phase difference $\Delta\phi'_{n_{\mathrm{R}},k}$ via frequency variations enables the current phase difference to be described as a summation of all past phase shifts, yielding

$$\Delta\phi_{n_{\mathrm{R}},k} = \sum_{\nu=1}^{k} 2\pi T_{\mathrm{S}} \Delta f_{n_{\mathrm{R}},\nu-1} + \Delta\phi'_{n_{\mathrm{R}},0}, \tag{7}$$

where $\Delta\phi'_{n_{\mathrm{R}},0}$ denotes the starting phase difference and the overall frequency difference

$$\Delta f_{n_{\mathrm{R}},k-1} = \Delta f'_{n_{\mathrm{R}}} + \frac{\Delta\phi'_{n_{\mathrm{R}},k} - \Delta\phi'_{n_{\mathrm{R}},k-1}}{2\pi T_{\mathrm{S}}} \tag{8}$$

accounts for both the slowly drifting beacon–RX frequency difference and the phase noise of both the beacon and the RX [32]. Since the proposed algorithm will estimate the phase and frequency difference in a recursive manner, the beacon–RX phase difference (7) at time step k is formulated recursively as

$$\Delta\phi_{n_{\mathrm{R}},k} = \Delta\phi_{n_{\mathrm{R}},k-1} + 2\pi T_{\mathrm{S}} \Delta f_{n_{\mathrm{R}},k-1}, \tag{9}$$

as in [33]. Inserting the beacon–RX phase difference $\Delta\phi_{n_{\mathrm{R}},k}$ in (6) into (5) yields

$$s_{\mathrm{BB},n_{\mathrm{R}},n_{\mathrm{A}},k} = A_{\mathrm{B}} a_{n_{\mathrm{R}},n_{\mathrm{A}}} \mathrm{e}^{\mathrm{j}\left(\Delta\phi_{n_{\mathrm{R}},k} - 2\pi f_{\mathrm{B}} \tau_{n_{\mathrm{R}},n_{\mathrm{A}},k}\right)}. \tag{10}$$

Evaluating the phase of (10) yields the measurement model $h_{n_\mathrm{R},n_\mathrm{A},k}$ at the n_Ath antenna of the n_Rth array as

$$\begin{aligned}\varphi_{n_\mathrm{R},n_\mathrm{A},k} &= h_{n_\mathrm{R},n_\mathrm{A},k}(\vec{p}_{\mathrm{B},k}, \Delta\phi_{n_\mathrm{R},k}) \\ &= \arg\left\{s_{\mathrm{BB},n_\mathrm{R},n_\mathrm{A},k}\right\} \\ &= \mathrm{mod}'_{2\pi}\left(\Delta\phi_{n_\mathrm{R},k} - 2\pi f_{\mathrm{B},k}\tau_{n_\mathrm{R},n_\mathrm{A},k}\right). \quad (11)\end{aligned}$$

Stacking the measured phases yields the measurement vector as

$$\begin{aligned}\vec{\varphi}_k &= \vec{h}(\vec{p}_{\mathrm{B},k}, \Delta\phi_{1,k}, \ldots, \Delta\phi_{N_\mathrm{R},k}) \\ &= \left(\cdots \vec{\varphi}^{\mathrm{T}}_{n_\mathrm{R},k} \cdots\right)^{\mathrm{T}} \quad (12)\end{aligned}$$

with the phases at one array

$$\vec{\varphi}_{n_\mathrm{R},k} = \left(\cdots \varphi_{n_\mathrm{R},n_\mathrm{A},k} \cdots\right)^{\mathrm{T}}. \quad (13)$$

B. MEASUREMENT NOISE MODEL

The phases, measured at spatially distributed antennas in indoor scenarios, are corrupted by many different error sources. In addition to the phase noise, which was introduced in Section II-A, thermal noise, multipath propagation, and unknown antenna phase characteristics disturb the measured phases. In indoor scenarios, the multipath propagation represents the main error source for localization systems [34]. However, Kalman filters minimize a least-squares metric [35] and, hence, the proposed QCHEKF treats multipath propagation as additive white Gaussian noise (AWGN), which impairs the phase measurements as

$$\vec{\varphi}_{\mathrm{meas},k} = \vec{\varphi}_k + \vec{w}_{\varphi,k}, \quad (14)$$

with $\vec{w}_{\varphi,k} \sim \mathcal{N}(\vec{0}, \sigma^2_\varphi \boldsymbol{I})$. In doing so, the AWGN model implies several assumptions on the measurement impairments. First, it assumes that the line-of-sight (LOS) is never blocked. Second, the AWGN model assumes that the impairments on the LOS signal are sufficiently small to neglect the non-linear distortion due to the phase extraction from the complex valued measurement data. Third, the AWGN model implicitly assumes the noise for different antennas to be uncorrelated, which is not true for multipath propagation. Therefore, it is advisable to decorrelate the LOS signal from the multipath propagation signal as much as possible by using widely spaced RX antennas [11], [36]. Further, the AWGN model implicitly assumes the noise for different time instances to be uncorrelated. Since the measurement errors caused by multipath propagation depend on the beacon's position, this is mainly valid for fast fading channels or a quickly moving beacon and, therefore, the proposed QCHEKF is most suited for tracking applications. Beside the uncorrelated noise assumption, (14) assumes normally distributed noise with constant power, which implies the complex valued measurements to be impaired by Gaussian distributed noise with constant signal-to-noise ratio [37]. This assumption is approximately valid, because both the multipath propagation receive power and the LOS signal power decrease with increasing beacon–RX distance.

Because of the phases' ambiguity, all phases are defined within $(-\pi, \pi]$ in this paper and, therefore, the noise term $\vec{w}_{\varphi,k}$ in (14) might cause a large difference between the measured $\vec{\varphi}_{\mathrm{meas},k}$ and the hypothetical phases $\vec{\varphi}_k$. Hence, the measurement deviation between the measured and correct phases must again be mapped to $(-\pi, \pi]$. Evaluating this deviation yields

$$\begin{aligned}&\mathrm{mod}'_{2\pi}\left(\vec{\varphi}_{\mathrm{meas},k} - \vec{\varphi}_k\right) \\ &= \mathrm{mod}'_{2\pi}\left(\mathrm{mod}'_{2\pi}\left(\vec{\varphi}_k + \vec{w}_{\varphi,k}\right) - \vec{\varphi}_k\right) \\ &= \mathrm{mod}'_{2\pi}\left(\vec{w}_{\varphi,k}\right) \\ &\approx \vec{w}_{\varphi,k}, \quad (15)\end{aligned}$$

which is valid as long as the noise standard deviation satisfies $\sigma_\varphi \ll \pi$. Despite the 2π-ambiguity, the noise shape in (14) is preserved within the deviation and, therefore, a Kalman filter based evaluation is well suited [38].

C. SYSTEM MODEL

Since the proposed algorithm mainly concerns the evaluation of phases, which are measured at spatially distributed antennas, arbitrary motion models can be incorporated. Most often, a constant velocity approach [39], such as

$$\begin{pmatrix} d_{\mathrm{B},k} \\ v_{\mathrm{B},d,k} \end{pmatrix} = \begin{pmatrix} 1 & T_\mathrm{S} \\ 0 & 1 \end{pmatrix} \begin{pmatrix} d_{\mathrm{B},k-1} \\ v_{\mathrm{B},d,k-1} \end{pmatrix} + \begin{pmatrix} T_\mathrm{S} \\ 1 \end{pmatrix} w_{v_d,k}, \quad (16)$$

where $d_{\mathrm{B},k} \in \{x_{\mathrm{B},k}, y_{\mathrm{B},k}, z_{\mathrm{B},k}\}$ is the beacon's position for each individual dimension, $v_{\mathrm{B},d,k} \in \{v_{\mathrm{B},x,k}, v_{\mathrm{B},y,k}, v_{\mathrm{B},z,k}\}$ denotes the beacon's velocity for each individual dimension, and $w_{v_d,k} \sim \mathcal{N}(0, \sigma^2_v)$ denotes the velocity noise, is well suited for localization purposes. Furthermore, the phase and frequency relation of the complete beacon–RX processing chain has to be modeled. In communications, digital phase locked loops (PLL) are used to provide a stable phase relation between a transmitter and a RX [40]. However, these PLLs also correct phase deviations caused by beacon movements, so the estimation of the phase and frequency relation between each beacon–RX pair has to be incorporated into the localization algorithm. Generally, PLLs can be well modeled via a Kalman filter, as in [33]. For this purpose, similar to the constant velocity concept, a constant frequency approach is established for each beacon–RX pair as

$$\begin{aligned}\begin{pmatrix} \Delta\phi_{n_\mathrm{R},k} \\ \Delta f_{n_\mathrm{R},k} \end{pmatrix} &= \begin{pmatrix} 1 & 2\pi T_\mathrm{S} \\ 0 & 1 \end{pmatrix} \begin{pmatrix} \Delta\phi_{n_\mathrm{R},k-1} \\ \Delta f_{n_\mathrm{R},k-1} \end{pmatrix} \\ &\quad + \begin{pmatrix} 2\pi T_\mathrm{S} \\ 1 \end{pmatrix} w_{\mathrm{RX},n_\mathrm{A},k} + \begin{pmatrix} 2\pi T_\mathrm{S} \\ 1 \end{pmatrix} w_{\mathrm{B},k}, \quad (17)\end{aligned}$$

where $w_{\mathrm{RX},n_\mathrm{A},k} \sim \mathcal{N}(0, \sigma^2_{n_\mathrm{A}})$ denotes the frequency noise at the n_Ath RX array and $w_{\mathrm{B},k} \sim \mathcal{N}(0, \sigma^2_\mathrm{B})$ denotes the beacon's frequency noise. In (17), the phase difference $\Delta\phi_{n_\mathrm{R},k-1}$ is created by the recursive summation of the past phase changes $2\pi T_\mathrm{S} \Delta f_{n_\mathrm{R},k-1}$, as in (9). Note that the beacon's frequency noise term is the same for all RXs. Stacking the beacon's position $d_{\mathrm{B},k}$ and velocity $v_{\mathrm{B},d,k}$ for every dimension, and the phase and frequency differences between each beacon–RX

pair, $\Delta\phi_{n_\mathrm{R},k}$ and $\Delta f_{n_\mathrm{R},k}$, yields the state vector $\vec{x}_k$ and the complete system state model as

$$\vec{x}_k = \boldsymbol{F}\vec{x}_{k-1} + \boldsymbol{G}\vec{w}_k, \tag{18}$$

where all phases are mapped to $(-\pi, \pi]$, and $\boldsymbol{F}$ denotes the state transition matrix, which models the relation between $\vec{x}_{k-1}$ and $\vec{x}_k$ according to (16) and (17). The system noise $\vec{w}_k \sim \mathcal{N}(\vec{0}, \boldsymbol{Q})$ in (18) includes all occurring system noise sources as $\vec{w}_k = (w_{v_x,k}\ w_{v_y,k}\ w_{v_z,k}\ w_{\mathrm{RX},1,k}, \cdots, w_{\mathrm{RX},N_\mathrm{A},k}\ w_{\mathrm{B},k})^\mathrm{T}$, which are mapped in (18) via the noise shaping matrix $\boldsymbol{G}$ onto the system state according to (16) and (17). Here, the covariance matrix $\boldsymbol{Q}$ contains the noise variances on the main diagonal according to the noise vector $\vec{w}_k$. Using the state vector $\vec{x}_k$, the measurement function in (12) is denoted as $\vec{h}(\vec{x}_k)$.

III. LOCALIZATION ALGORITHM

Because both the measurement deviation and the system noise are assumed to be normally distributed, an extended Kalman filter (EKF) based evaluation is well suited [38]. The EKF works in a recursive predict-update manner, which will be examined in the following section. Here, $(\cdot)_{k|k}$ denotes an estimate at time step k and $(\cdot)_{k|k-1}$ denotes the estimate at time step k after the prediction step, meaning that the measurements at time step k have so far not been incorporated.

A. PREDICTION STEP

The prediction step performs a linear extrapolation of the current system state, see [41]. Despite the phase ambiguity, the prediction step remains unchanged in comparison to a standard EKF, which yields

$$\begin{aligned} \vec{x}_{k|k-1} &= \boldsymbol{F}\vec{x}_{k-1|k-1}, \\ \boldsymbol{P}_{k|k-1} &= \boldsymbol{F}\boldsymbol{P}_{k-1|k-1}\boldsymbol{F}^\mathrm{T} + \boldsymbol{G}\boldsymbol{Q}\boldsymbol{G}^\mathrm{T}. \end{aligned} \tag{19}$$

For consistency, all phases should again be mapped to $(-\pi, \pi]$.

B. PHASE PREPROCESSING

Generally, the algorithm's concept is to evaluate both the phase differences between the antennas, which yield absolute information about the beacon's position, and the absolute phases, which provide highly accurate relative information about the beacon's position. To calculate suitable phase differences and choose one absolute phase, the phases at each array are preprocessed using a matrix $\boldsymbol{T}_{\mathrm{pre},n_\mathrm{R}}$ as

$$\vec{\varphi}^{\,\mathrm{pre}}_{n_\mathrm{R},k} = \boldsymbol{T}_{\mathrm{pre},n_\mathrm{R}}\vec{\varphi}_{n_\mathrm{R},k}, \tag{20}$$

where the preprocessing matrix $\boldsymbol{T}_{\mathrm{pre},n_\mathrm{R}}$ evaluates $N_{\mathrm{A},n_\mathrm{R}} - 1$ phase differences between antenna pairs per array via the first $N_{\mathrm{A},n_\mathrm{R}} - 1$ rows, and the absolute phase at one antenna per array via the last row. To assure that all antennas' phase information is incorporated, $\boldsymbol{T}_{\mathrm{pre},n_\mathrm{R}}$ needs to have full rank. Hence, the evaluated phase differences should create a spanning tree between all antennas of the array [42] to assure a full rank of the first $N_{\mathrm{A},n_\mathrm{R}} - 1$ rows of $\boldsymbol{T}_{\mathrm{pre},n_\mathrm{R}}$. Since the phase difference unambiguity range of an evaluated antenna pair increases with decreasing antenna distance, it is advisable to choose the evaluated phase differences in $\boldsymbol{T}_{\mathrm{pre},n_\mathrm{R}}$ so that each receive antenna is connected to the spanning tree via the most closely spaced neighboring antenna. By stacking the preprocessing matrices $\boldsymbol{T}_{\mathrm{pre},n_\mathrm{R}}$ of each array, the complete preprocessing matrix $\boldsymbol{T}_\mathrm{pre}$ evaluates the measured phases as

$$\vec{\varphi}^{\,\mathrm{pre}}_{\mathrm{meas},k} = \boldsymbol{T}_\mathrm{pre}\vec{\varphi}_{\mathrm{meas},k}. \tag{21}$$

With

$$\begin{aligned} &\mathrm{mod}'_{2\pi}\left(\boldsymbol{T}_\mathrm{pre}\vec{\varphi}_{\mathrm{meas},k} - \boldsymbol{T}_\mathrm{pre}\vec{\varphi}_k\right) \\ &= \mathrm{mod}'_{2\pi}\left(\boldsymbol{T}_\mathrm{pre}\vec{w}_{\varphi,k}\right) \\ &\approx \boldsymbol{T}_\mathrm{pre}\vec{w}_{\varphi,k}, \end{aligned} \tag{22}$$

the measurement deviation remains normally distributed for $\sigma_\varphi \ll \pi$. Hence, the measurement error of the preprocessed phase is normally distributed as $\boldsymbol{T}_\mathrm{pre}\vec{w}_{\varphi,k} \sim \mathcal{N}(\vec{0}, \boldsymbol{R}_\mathrm{pre} = \sigma_\varphi^2\boldsymbol{T}_\mathrm{pre}\boldsymbol{T}_\mathrm{pre}^\mathrm{T})$. The preprocessed residual $\vec{r}$ between the measured phases and the hypothetical phases is then given by

$$\vec{r}(\vec{x}_k) = \mathrm{mod}'_{2\pi}\left(\boldsymbol{T}_\mathrm{pre}\vec{\varphi}_{\mathrm{meas},k} - \boldsymbol{T}_\mathrm{pre}\vec{h}(\vec{x}_k)\right). \tag{23}$$

C. UPDATE STEP

Generally, the EKF update step minimizes a generalized least squares metric [21], [35], incorporating both the measurement and the predicted system state. By linearizing and minimizing the likelihood function

$$\begin{aligned} J(\vec{x}_k) = \ &\frac{1}{2}\vec{r}^\mathrm{T}(\vec{x}_k)\boldsymbol{R}_\mathrm{pre}^{-1}\vec{r}(\vec{x}_k) \\ &+\frac{1}{2}(\vec{x}_k - \vec{x}_{k|k-1})^\mathrm{T}\boldsymbol{P}_{k|k-1}^{-1}(\vec{x}_k - \vec{x}_{k|k-1}) \end{aligned} \tag{24}$$

starting from $\vec{x}_{k|k-1}$, the update step

$$\begin{aligned} \boldsymbol{K}_k &= \boldsymbol{P}_{k|k-1}\boldsymbol{H}_{\mathrm{pre},k}^\mathrm{T}\left(\boldsymbol{H}_{\mathrm{pre},k}\boldsymbol{P}_{k|k-1}\boldsymbol{H}_{\mathrm{pre},k}^\mathrm{T} + \boldsymbol{R}_\mathrm{pre}\right)^{-1}, \\ \vec{\varphi}^{\,\mathrm{pre}}_{\mathrm{meas},k} &= \boldsymbol{T}_\mathrm{pre}\vec{\varphi}_{\mathrm{meas},k}, \\ \vec{x}_{k|k} &= \vec{x}_{k|k-1} + \boldsymbol{K}_k\mathrm{mod}'_{2\pi}\left(\vec{\varphi}^{\,\mathrm{pre}}_{\mathrm{meas},k} - \boldsymbol{T}_\mathrm{pre}\vec{h}(\vec{x}_{k|k-1})\right), \\ \boldsymbol{P}_{k|k} &= (\boldsymbol{I} - \boldsymbol{K}_k\boldsymbol{H}_{\mathrm{pre},k})\boldsymbol{P}_{k|k-1}, \end{aligned} \tag{25}$$

is established as shown in the appendix, where $\boldsymbol{H}_{\mathrm{pre},k} = \boldsymbol{T}_\mathrm{pre}\boldsymbol{H}_k$ holds, with $\boldsymbol{H}_k$ denoting the Jacobian of $\vec{h}(\vec{x}_k)$ at $\hat{\vec{x}}_{k|k-1}$, and $\boldsymbol{K}_k$ denoting the Kalman gain. Here, the difference to the common EKF is the $\mathrm{mod}'_{2\pi}(\cdot)$ mapping of the phase error. This is valid as long as the absolute differences between the measured $\vec{\varphi}_{\mathrm{meas},k}$ and the hypothetical phases $\vec{h}(\vec{x}_{k|k-1})$ do not exceed π, which is also a direct result of the update step derivation in the appendix.

D. INTERPRETATION

In [23], a HEKF was proposed that estimates the position of an incoherent beacon. To cope with the incoherent measurement process, the HEKF in [23] evaluated only phase differences. In this paper, the novel QCHEKF extends this concept by additionally evaluating absolute phases, because these are much more sensitive to position changes, and enable further improvement of localization accuracy in comparison to a pure phase difference evaluation. For this purpose,

the absolute phase differences between the beacon and each RX $\Delta\phi_{n_R,k}$ have to be estimated. Assuming the absolute phase behavior to be completely unknown, that is $\sigma^2_{n_A} \to \infty$ and/or $\sigma^2_B \to \infty$, the same localization accuracy as in [23] is achieved. If the frequency differences $\Delta f_{n_R,k}$ remain sufficiently stable, the QCHEKF is able to estimate the absolute phase and frequency relation between each beacon–RX pair by comparing the phase-difference based position estimation with the absolute phase measurements. Thereafter, when the phase and frequency relation is estimated with sufficient accuracy, the QCHEKF is able to incorporate the absolute phase measurements in the localization process, further increasing the localization accuracy. For a reliable localization based on the evaluation of absolute phases, a high update rate is necessary to ensure that the absolute differences between the measured $\vec{\varphi}_{\text{meas},k}$ and the hypothetical phases $\vec{h}(\vec{x}_{k|k-1})$ at the predicted position remain less than π. Otherwise, a position update towards an incorrect position will occur. Assuming the phase noise to be small, the main phase shifts occur because of position changes. Unfortunately, the exact behavior of the predicted position is difficult to analyze for every situation and, therefore, we suggest choosing the maximum position difference between successive measurement instances to be significantly less than half of the wavelength. Note that the absolute position estimation is still performed only based on the phase differences and, hence, the QCHEKF still provides accurate estimates for larger position deviations. Thus, in the event of an erroneous position estimation, which is related to the ambiguity of the evaluated absolute phases, the algorithm can slowly correct the error by adopting the beacon–RX phase difference $\Delta\phi_{n_R,k}$.

E. INITIALIZATION

Generally, Kalman filters exponentially converge toward the system state after the initialization [43]. In the beginning, the system state varies widely until the steady state is reached. This procedure is well suited to estimate the position and velocity for a pure phase difference evaluation, because phase differences provide a sufficiently ambiguous range [23]. However, as discussed in the previous subsection, the evaluation of absolute phase measurements requires the absolute differences between the measured $\vec{\varphi}_{\text{meas},k}$ and the hypothetical phases $\vec{h}(\vec{x}_{k|k-1})$ at the predicted position to be less than π, which contradicts strong variations in the position estimate after initialization.

Hence, we propose starting the QCHEKF in a HEKF-based manner, meaning that only the phase differences are evaluated. For this purpose, coarse pre-estimates of the beacon's position $\vec{p}_{B,0}$ and frequency $f_{B,0}$ are assumed. To exclude the absolute phases of the beacon-RX pairs from the localization process in the beginning, the frequency variation is assumed to be completely random in each sample via $\sigma^2_{n_A} \to \infty$ and/or $\sigma^2_B \to \infty$. Then, the localization is conducted as for a pure phase difference-based HEKF, while the frequency and phase relations are estimated. To start the QCHEKF, the variances $\sigma^2_{n_A}$ and/or σ^2_B are set to their desired values. Since the beacon's position and velocity are already roughly estimated, the QCHEKF then incorporates the relative phase and frequency relations, thereby increasing the localization accuracy.

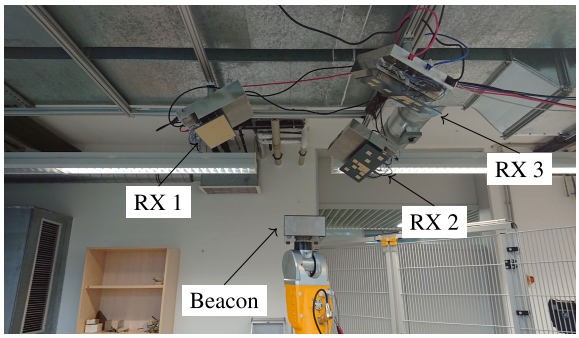

FIGURE 3. Measurement setup consisting of three receiving arrays, each with 12 antennas, and one beacon, which is mounted on a robotic arm and emits a 24 GHz signal using one antenna.

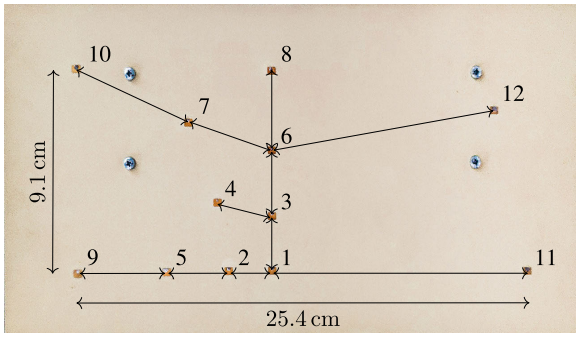

FIGURE 4. Array RX 1, measuring the phases at 12 patch antennas, which are spread over an area of 25.4 cm × 9.1 cm. The arrows between antenna pairs depict the spanning tree of the evaluated phase differences in T_{pre,n_R}. The antenna geometry was optimized for an efficient HEKF-based phase difference evaluation.

IV. EXPERIMENTAL VERIFICATION

In this section, localization measurements within the 24 GHz industrial, scientific, and medical (ISM) band are presented. First, the measurement setup is described. Then, localization results are shown and analyzed.

A. MEASUREMENT SETUP

The measurements are conducted within the setup shown in Fig. 3. Because of the strong reflectors in the surrounding, the considered environment depicts a challenging multipath scenario. The measurement setup consists of $N_R = 3$ identical receivers, each with $N_{A,n_R} = 12$ antennas, and one beacon, which is mounted on a robotic arm. The antenna geometry of each array with an aperture size of 25.4 cm × 9.1 cm and the phase differences, which are evaluated by $\boldsymbol{T}_{\text{pre},n_R}$, are shown in Fig. 4. To incorporate absolute phase measurements, the last row of $\boldsymbol{T}_{\text{pre},n_R}$ evaluates the absolute phase measurement at antenna 1. The beacon's 24 GHz signal is created via a voltage-controlled oven-controlled 50 MHz crystal oscillator (VCOCXO) with the use of a PLL. According to the data sheet, the oscillator provides a 10 s Allan

deviation of approximately $4 \cdot 10^{-11}$, which corresponds to a frequency change of approximately 1 Hz after 10 s for the 24 GHz CW signal. Note that the behavior is degraded due to the acceleration force of the robotic arm [44]. At the RXs, the received signals are converted to a low intermediate frequency by mixing with slightly shifted 24 GHz signals, which are created by the identical VCOCXOs and PLLs as used for the beacon. To compensate for phase mismatch, coupling, and antenna position errors, the arrays have been calibrated in-situ with 50 measurements at known positions using the calibration concept proposed in [45]. Unfortunately, the robotic arm is able to provide highly accurate positioning, but not corresponding timing information when it performs continuous movements. Therefore, a direct comparison of the correct and the estimated beacon positions is not possible and only the distance between the estimated beacon positions to the overall trajectory can be evaluated here.

B. MEASUREMENT RESULTS

To assess the QCHEKF, the localization results are compared to the results of a pure phase difference HEKF. Since $\boldsymbol{T}_{\text{pre},n_\text{R}}$ evaluates $N_{\text{A},n_\text{R}}-1$ phase differences and one absolute phase via the last row, a pure phase difference HEKF is obtained by removing the last row of $\boldsymbol{T}_{\text{pre},n_\text{R}}$ and omitting the constant frequency part in the system model. During the measurement, the robotic arm is moved continuously along a trajectory $\vec{p}_\text{rob}(t)$, which consists of 21 straight sections at a constant height with a total trajectory length of 2.2 m, as shown in Fig. 5-7. While the trajectory parts with a linear motion are well suited for tracking systems, the changes of direction contradict the constant velocity model in (16) and are challenging for tracking systems. The complete measurement time was approximately 26 s, yielding measurements at 37,523 time instances, which corresponds to an update rate of 1.4 kHz.

Typically, the localization errors are calculated by directly comparing the estimated positions with reference positions. However, since an exact time synchronization of the robotic arm is not possible, each position estimate can only be assessed via its minimal deviation from the trajectory as

$$d_{\text{min},k} = \min_t \left\| \hat{\vec{p}}_{\text{B},k} - \vec{p}_\text{rob}(t) \right\|_2 . \tag{26}$$

Hence, a root mean square error can be defined as

$$\text{RMSE} = \sqrt{\frac{\sum_k d_{\text{min},k}^2}{K}}, \tag{27}$$

where K is the number of position estimations. The resulting RMSE can be interpreted as a 2D RMSE of a 3D localization process, because it most often depicts the 2D trajectory–beacon distance in the plane, which is orthogonal to the straight line currently driven by the robotic arm. Besides the RMSE, the maximal distance from the trajectory

$$d_\text{max} = \max_k d_{\text{min},k} \tag{28}$$

is used to assess the localization results.

TABLE 1. Used QCHEKF and HEKF parameters for all presented measurement evaluations.

	HEKF	QCHEKF
Start position $d_{\text{B},0}$ (m)	Reference	Reference
Start speed $v_{\text{B},d,0}$ $(\frac{m}{s})$	0	0
Start frequency deviation $\Delta f_{n_\text{R},0}$ (Hz)	0	0
Start phase deviation $\Delta\varphi_{n_\text{R},0}$ $(^\circ)$	0	0
Start covariance matrix $\boldsymbol{P}_{0\|0} = \sigma_P \boldsymbol{I}$	$\sigma_P \to \infty$	$\sigma_P \to \infty$
Measurement noise σ_φ $(^\circ)$	5	5
Velocity noise σ_v $(\frac{\text{m}}{\text{s}})$	$5.1 \cdot 10^{-5}$	$5.1 \cdot 10^{-5}$
Frequency noise $\sigma_{n_\text{A}} = \sigma_\text{B}$ (Hz), $k < 10$	not used	$\to \infty$
Frequency noise $\sigma_{n_\text{A}} = \sigma_\text{B}$ (Hz), $k \geq 10$	not used	$3.6 \cdot 10^{-4}$

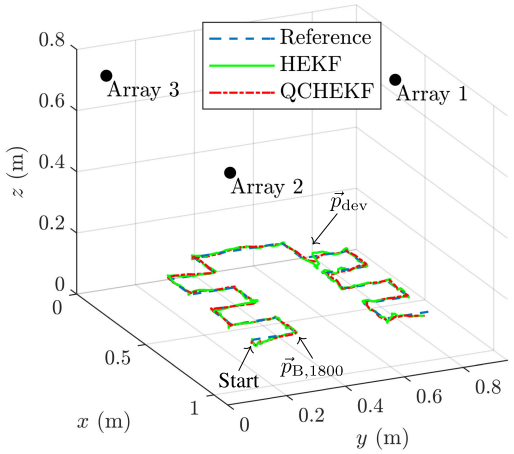

FIGURE 5. QCHEKF and HEKF localization result using 12 antennas, yielding an array size of 25.4 cm × 9.1 cm.

To use the HEKF and QCHEKF, several parameters, summarized in Table 1, have to be chosen. Despite the beacon's position, which is known via the reference, the system states are unknown and initialized by zeros. The corresponding covariance matrices of the HEKF and the QCHEKF are initialized via a diagonal matrix with large entries to reflect a high uncertainty about the system state at the beginning. The used noise parameters were estimated by hand and are held constant for all subsequent evaluations. First, the values for $\sigma_\varphi = 5^\circ$ and $\sigma_v \approx 5.1 \cdot 10^{-5} \frac{\text{m}}{\text{s}}$ were chosen so that the HEKF's performance was optimized. Afterwards, $\sigma_{n_\text{A}} = \sigma_\text{B} \approx 3.6 \cdot 10^{-4}$ Hz was determined so that the QCHEKF's performance was optimized. As discussed in Section III-E, the QCHEKF starts to involve the phase frequency relation with the tenth measurement instance by setting $\sigma_{n_\text{A}} = \sigma_\text{B} = 3.6 \cdot 10^{-4}$ Hz.

By evaluating the HEKF and QCHEKF using all 12 antennas at all receivers with an aperture of 25.4 cm × 9.1 cm, the localization results in Fig. 5 are obtained. The standard HEKF already provides very accurate localization results

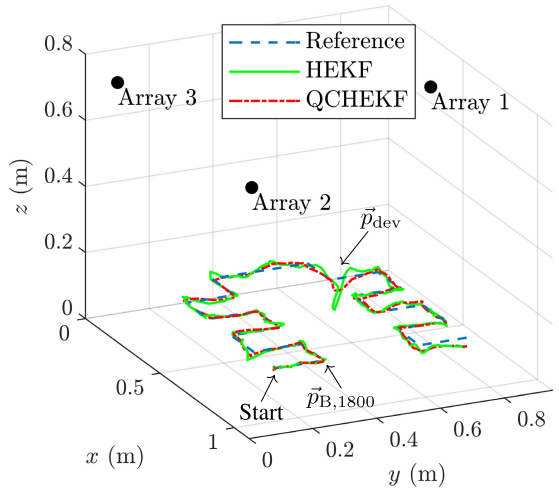

FIGURE 6. QCHEKF and HEKF localization result using antennas 1-8, yielding an array size of 6 cm × 9.1 cm.

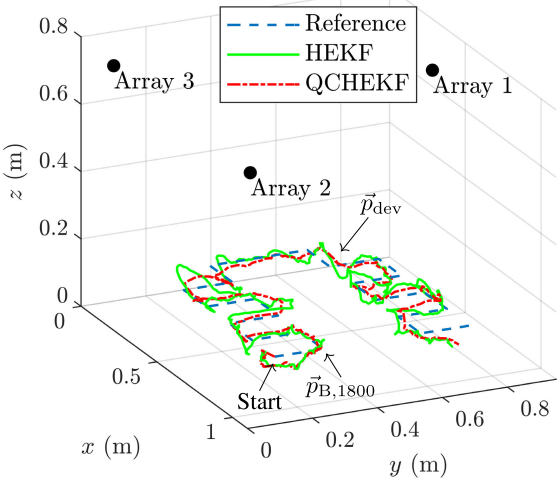

FIGURE 7. QCHEKF and HEKF localization result using antennas 1-3, yielding an array size of 2.5 cm × 2.5 cm.

with RMSE ≈ 0.78 cm. Note that the filter requires some time to converge, so the localization results are evaluated starting with the 1800th sample at approximately the first change in direction at $\vec{p}_{\mathrm{B},1800} \approx [0.85\,\mathrm{m}, 0.35\,\mathrm{m}, 0.10\,\mathrm{m}]^{\mathrm{T}}$. However, while the constant velocity model is well suited for the straight trajectory sections, it struggles whenever changes of direction occur. Then, the constant velocity model is not able to compensate for localization errors, which most often occur because of multipath propagation. The effect is most visible at $\vec{p}_{\mathrm{dev}} = [0.25\,\mathrm{m}, 0.65\,\mathrm{m}, 0.10\,\mathrm{m}]$. This causes a maximal error of $d_{\max} \approx 5.0\,\mathrm{cm}$. In comparison, the QCHEKF is able to trace the changes of direction, reducing the maximum error to $d_{\max} \approx 1.6\,\mathrm{cm}$ and improving the accuracy to RMSE ≈ 0.51 cm. The cumulative error function is shown in Fig. 8. It can be observed that the QCHEKF improves the localization accuracy whenever the

TABLE 2. Comparison of the localization results for the different presented measurement evaluations.

	HEKF		QCHEKF	
	RMSE	$d_{\max}$	RMSE	$d_{\max}$
Antennas 1-12	0.78 cm	5.0 cm	0.51 cm	1.6 cm
Antennas 1-8	1.3 cm	8.7 cm	0.9 cm	3.4 cm
Antennas 1-3	3.0 cm	7.6 cm	2.2 cm	5.1 cm

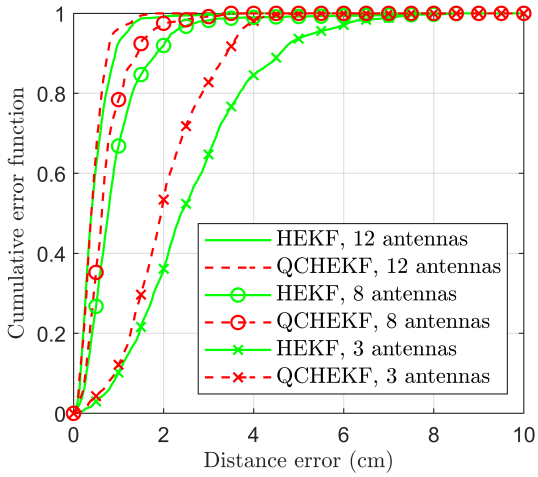

FIGURE 8. Cumulative error distribution function for the different evaluation cases and algorithms.

HEKF yields high errors due to stability issues induced by model errors.

The accuracy of the standard HEKF mainly depends on the array size and beacon distance, because these parameters directly influence the phase difference measurement sensitivity [11]. Hence, the HEKF's accuracy decreases for smaller arrays. By only evaluating the phase differences of antennas 1-8 in Fig. 4 at all arrays, the array size is reduced to 6 cm×9.1 cm, yielding the localization results in Fig. 6. Then, the HEKF's accuracy decreases to RMSE ≈ 1.3 cm and the maximum error increases to $d_{\max} \approx 8.7\,\mathrm{cm}$. In comparison, the QCHEKF yields RMSE ≈ 0.9 cm and $d_{\max} \approx 3.4\,\mathrm{cm}$. The cumulative error function in Fig. 8 again validates the QCHEKF's ability to prevent high localization errors.

By reducing the array's evaluated antennas to 1-3, which is the minimum for a 2D array, an array of size 2.5 cm × 2.5 cm is obtained. Now, the HEKF has difficulties reconstructing the driven trajectory, as shown in Fig. 7, yielding RMSE ≈ 3.0 cm and $d_{\max} \approx 7.6\,\mathrm{cm}$. In comparison to the localization result with eight antennas per array, the maximum distance error is slightly reduced, because of the smaller error at $\vec{p}_{\mathrm{dev}}$. Overall, many large errors occur, as can be observed from the cumulative error function in Fig. 8. The QCHEKF improves the localization accuracy to RMSE ≈ 2.2 cm and $d_{\max} \approx 5.1\,\mathrm{cm}$, and effectively prevents the high localization errors in the cumulative error function in Fig. 8.

The RMSEs and maximal deviations of the different measurement evaluations are summarized in Table 2. Generally, the measurements have shown that the QCHEKF is

able to improve the localization accuracy compared to the HEKF, particularly when the HEKF's localization performance deteriorates due to multipath propagation or a deficient motion model. Visible in the cumulative error function in Fig. 8, the potential improvement increases for smaller arrays, because the phase differences become less sensitive to position changes [11], whereas the sensitivity of absolute phases does not scale with the array size. Hence, even in the three-antenna case in Fig. 7, the QCHEKF provides very accurate information about relative movements. This can be seen by inspecting the localization behavior during the changes of direction, where the HEKF's phase difference evaluation results in large localization errors.

V. CONCLUSION

In this paper, the novel QCHEKF was presented, which incorporates the evaluation of absolute phase measurements into incoherent PDOA localization systems to enable highly accurate beacon tracking. Particularly relative motions can be tracked precisely, enabling, for example, the detection of a person's tremor or mechanical vibrations. In comparison to the UWB systems, the simultaneous tracking of many targets is easily implementable via slightly frequency-shifted beacons. The QCHEKF's localization accuracy depends on the stability of the frequency references used. Therefore, the relationship between the oscillator's frequency stability and the localization accuracy should be studied in future research. Localization accuracy could be improved further by sharing the signal of a common oscillator to all receivers, each with an individual PLL, and adopting the QCHEKF's system accordingly. In this paper, the QCHEKF relies on the evaluation of the permanently available LOS between the beacon and each receiver. To extend the QCHEKF for the varying conditions in complex indoor measurement setups, a detection of non-LOS scenarios, for example by an adaptive noise estimation [46], is desirable.

APPENDIX

In this appendix, (24) is minimized using one Newton step [47] beginning at the state prediction $\vec{x}_{k|k-1}$. For this purpose, $\vec{r}(\vec{x}_k)$ is Taylor expanded at $\vec{x}_{k|k-1}$ as

$$\begin{aligned}
&\vec{r}(\vec{x}_k)\\
&\quad= \mathrm{mod}'_{2\pi}\left(\boldsymbol{T}_{\mathrm{pre}}\vec{\varphi}_{\mathrm{meas},k} - \boldsymbol{T}_{\mathrm{pre}}\vec{h}(\vec{x}_k)\right)\\
&\quad\approx \mathrm{mod}'_{2\pi}\left(\boldsymbol{T}_{\mathrm{pre}}\vec{\varphi}_{\mathrm{meas},k} - \boldsymbol{T}_{\mathrm{pre}}\left(\vec{h}(\vec{x}_{k|k-1}) + \boldsymbol{H}_k\Delta\vec{x}_k\right)\right)\\
&\quad= \vec{r}(\vec{x}_{k|k-1}) - \boldsymbol{H}_{\mathrm{pre},k}\Delta\vec{x}_k \qquad (29)
\end{aligned}$$

which is valid as long as the absolute differences between the measured and the hypothetical phases do not exceed π, and where $\Delta\vec{x}_k = \vec{x}_k - \vec{x}_{k|k-1}$ holds. Inserting (29) in (24) yields

$$\begin{aligned}
J(\vec{x}_k) \approx\ & \frac{1}{2}(\vec{r}(\vec{x}_{k|k-1}) - \boldsymbol{H}_{\mathrm{pre},k}\Delta\vec{x}_k)^{\mathrm{T}}\boldsymbol{R}_{\mathrm{pre}}^{-1}\\
&\cdot(\vec{r}(\vec{x}_{k|k-1}) - \boldsymbol{H}_{\mathrm{pre},k}\Delta\vec{x}_k) + \frac{1}{2}\Delta\vec{x}_k^{\mathrm{T}}\boldsymbol{P}_{k|k-1}^{-1}\Delta\vec{x}_k. \qquad (30)
\end{aligned}$$

The gradient of (30) is given by

$$\begin{aligned}
&\mathrm{grad}(J(\vec{x}_k))\\
&\quad= -\boldsymbol{H}_{\mathrm{pre},k}^{\mathrm{T}}\boldsymbol{R}_{\mathrm{pre}}^{-1}\left(\vec{r}_k(\vec{x}_{k|k-1}) - \boldsymbol{H}_{\mathrm{pre},k}\Delta\vec{x}_k\right) + \boldsymbol{P}_{k|k-1}^{-1}\Delta\vec{x}_k\\
&\quad= -\boldsymbol{H}_{\mathrm{pre},k}^{\mathrm{T}}\boldsymbol{R}_{\mathrm{pre}}^{-1}\vec{r}_k(\vec{x}_{k|k-1}) - \boldsymbol{H}_{\mathrm{pre},k}^{\mathrm{T}}\boldsymbol{R}_{\mathrm{pre}}^{-1}\boldsymbol{H}_{\mathrm{pre},k}\vec{x}_{k|k-1}\\
&\qquad-\boldsymbol{P}_{k|k-1}^{-1}\vec{x}_{k|k-1} + (\boldsymbol{P}_{k|k-1}^{-1} + \boldsymbol{H}_{\mathrm{pre},k}^{\mathrm{T}}\boldsymbol{R}_{\mathrm{pre}}^{-1}\boldsymbol{H}_{\mathrm{pre},k})\vec{x}_k. \qquad (31)
\end{aligned}$$

Evaluating $\mathrm{grad}(J(\vec{x}_k))_{\vec{x}_k} \stackrel{!}{=} \vec{0}$ yields the state vector estimate as

$$\begin{aligned}
\vec{x}_{k|k} =\ & \left(\boldsymbol{H}_{\mathrm{pre},k}^{\mathrm{T}}\boldsymbol{R}_{\mathrm{pre}}^{-1}\boldsymbol{H}_{\mathrm{pre},k} + \boldsymbol{P}_{k|k-1}^{-1}\right)^{-1}\left(\boldsymbol{P}_{k|k-1}^{-1}\vec{x}_{k|k-1}\right.\\
&\left.+\boldsymbol{H}_{\mathrm{pre},k}^{\mathrm{T}}\boldsymbol{R}_{\mathrm{pre}}^{-1}\left(\vec{r}(\vec{x}_{k|k-1}) + \boldsymbol{H}_{\mathrm{pre},k}\vec{x}_{k|k-1}\right)\right)\\
=\ & \vec{x}_{k|k-1} + \boldsymbol{K}_k\vec{r}(\vec{x}_{k|k-1}), \qquad (32)
\end{aligned}$$

with

$$\begin{aligned}
\boldsymbol{K}_k =\ & \left(\boldsymbol{H}_{\mathrm{pre},k}^{\mathrm{T}}\boldsymbol{R}_{\mathrm{pre}}^{-1}\boldsymbol{H}_{\mathrm{pre},k} + \boldsymbol{P}_{k|k-1}^{-1}\right)^{-1}\boldsymbol{H}_{\mathrm{pre},k}^{\mathrm{T}}\boldsymbol{R}_{\mathrm{pre}}^{-1}\\
=\ & \boldsymbol{P}_{k|k-1}\boldsymbol{H}_{\mathrm{pre},k}^{\mathrm{T}}\left(\boldsymbol{H}_{\mathrm{pre},k}\boldsymbol{P}_{k|k-1}\boldsymbol{H}_{\mathrm{pre},k}^{\mathrm{T}} + \boldsymbol{R}_{\mathrm{pre}}\right)^{-1}, \qquad (33)
\end{aligned}$$

and

$$\left(\boldsymbol{H}_{\mathrm{pre},k}^{\mathrm{T}}\boldsymbol{R}_{\mathrm{pre}}^{-1}\boldsymbol{H} + \boldsymbol{P}_{k|k-1}^{-1}\right)^{-1} = (\boldsymbol{I} - \boldsymbol{K}_k\boldsymbol{H}_{\mathrm{pre},k})\boldsymbol{P}_{k|k-1}, \quad (34)$$

as in [35]. Since the covariance matrix of a Gaussian distribution is equivalent to the inverse Hessian matrix of the likelihood function [41], the inverse Hessian of (30) is evaluated as

$$\begin{aligned}
\boldsymbol{P}_{k|k} =\ & \left(\boldsymbol{H}_{\mathrm{pre},k}^{\mathrm{T}}\boldsymbol{R}_{\mathrm{pre}}^{-1}\boldsymbol{H}_{\mathrm{pre},k} + \boldsymbol{P}_{k|k-1}^{-1}\right)^{-1}\\
=\ & \left(\boldsymbol{I} - \boldsymbol{K}_k\boldsymbol{H}_{\mathrm{pre},k}\right)\boldsymbol{P}_{k|k-1} \qquad (35)
\end{aligned}$$

as in [35], where again, (34) was used.

REFERENCES

[1] M. Vossiek, L. Wiebking, P. Gulden, J. Wieghardt, C. Hoffmann, and P. Heide, "Wireless local positioning," *IEEE Microw. Mag.*, vol. 4, no. 4, pp. 77–86, Dec. 2003.

[2] H. Hile and G. Borriello, "Positioning and orientation in indoor environments using camera phones," *IEEE Comput. Graph. Appl.*, vol. 28, no. 4, pp. 32–39, Jul. 2008.

[3] C. Medina, J. C. Segura, and A. De la Torre, "Ultrasound indoor positioning system based on a low-power wireless sensor network providing sub-centimeter accuracy," *Sensors*, vol. 13, no. 3, pp. 3501–3526, 2013, [Online]. Available: https://www.mdpi.com/1424-8220/13/3/3501

[4] M. Hehn, E. Sippel, C. Carlowitz, and M. Vossiek, "High-accuracy localization and calibration for 5-DoF indoor magnetic positioning systems," *IEEE Trans. Instrum. Meas.*, vol. 68, no. 10, pp. 4135–4145, Oct. 2019.

[5] P. Zhang, J. Lu, Y. Wang, and Q. Wang, "Cooperative localization in 5G networks: A survey," *ICT Exp.*, vol. 3, no. 1, pp. 27–32, Mar. 2017. [Online]. Available: http://www.sciencedirect.com/science/article/pii/S2405959517300346

[6] X. Li, "Collaborative localization with received-signal strength in wireless sensor networks," *IEEE Trans. Veh. Technol.*, vol. 56, no. 6, pp. 3807–3817, Nov. 2007.

[7] K. Ullah, I. V. Custodio, N. Shah, and E. D. S. Moreira, "An experimental study on the behavior of received signal strength in indoor environment," in *Proc. 11th Int. Conf. Frontiers Inf. Technol.*, Dec. 2013, pp. 259–264.

[8] X. Ye, X. Yin, X. Cai, A. P. Yuste, and H. Xu, "Neural-network-assisted UE localization using radio-channel fingerprints in LTE networks," *IEEE Access*, vol. 5, pp. 12071–12087, 2017.

[9] X. Wang, L. Gao, S. Mao, and S. Pandey, "CSI-based fingerprinting for indoor localization: A deep learning approach," *IEEE Trans. Veh. Technol.*, vol. 66, no. 1, pp. 763–776, Jan. 2017.

[10] S. R. Jondhale and R. S. Deshpande, "Kalman filtering framework-based real time target tracking in wireless sensor networks using generalized regression neural networks," *IEEE Sensors J.*, vol. 19, no. 1, pp. 224–233, Jan. 2018.
[11] E. Sippel, J. Geiss, S. Bruckner, P. Groschel, M. Hehn, and M. Vossiek, "Exchanging bandwidth with aperture size in wireless indoor localization–or why 5G/6G systems with antenna arrays can outperform UWB solutions," *IEEE Open J. Veh. Technol.*, vol. 2, pp. 207–217, May 2021.
[12] M. R. Mahfouz, C. Zhang, B. C. Merkl, M. J. Kuhn, and A. E. Fathy, "Investigation of high-accuracy indoor 3-D positioning using UWB technology," *IEEE Trans. Microw. Theory Techn.*, vol. 56, no. 6, pp. 1316–1330, Jun. 2008.
[13] C. Zhang, M. J. Kuhn, B. C. Merkl, A. E. Fathy, and M. R. Mahfouz, "Real-time noncoherent UWB positioning radar with millimeter range accuracy: Theory and experiment," *IEEE Trans. Microw. Theory Techn.*, vol. 58, no. 1, pp. 9–20, Jan. 2010.
[14] M. J. Kuhn, M. R. Mahfouz, J. Turnmire, Y. Wang, and A. E. Fathy, "A multi-tag access scheme for indoor UWB localization systems used in medical environments," in *Proc. IEEE Topical Conf. Biomed. Wireless Technol., Netw., Sens. Syst.*, Jan. 2011, pp. 75–78.
[15] R. Bharadwaj, C. G. Parini, and A. Alomainy, "Experimental investigation of 3-D human body localization using wearable ultra-wideband antennas," *IEEE Trans. Antennas Propag.*, vol. 63, no. 11, pp. 5035–5044, Nov. 2015.
[16] A. R. J. Ruiz and F. S. Granja, "Comparing ubisense, bespoon, and decawave UWB location systems: Indoor performance analysis," *IEEE Trans. Instrum. Meas.*, vol. 66, no. 8, pp. 2106–2117, Aug. 2017.
[17] A. Badawy, T. Khattab, D. Trinchero, T. ElFouly, and A. Mohamed, "A simple angle of arrival estimation system," in *Proc. IEEE Wireless Commun. Netw. Conf. (WCNC)*, Mar. 2017, pp. 1–6.
[18] A. B. Miller and B. M. Miller, "Underwater target tracking using bearing-only measurements," *J. Commun. Technol. Electron.*, vol. 63, no. 6, pp. 643–649, Jun. 2018, doi: 10.1134/S1064226918060207.
[19] M. Lipka, E. Sippel, M. Hehn, J. Adametz, M. Vossiek, Y. Dobrev, and P. Gulden, "Wireless 3D localization concept for industrial automation based on a bearings only extended Kalman filter," in *Proc. Asia–Pacific Microw. Conf. (APMC)*, Nov. 2018, pp. 821–823.
[20] R. R. Moawad, H. Nofal, and M. I. Dessouky, "Study a bearing-only moving ground target tracking problem using single seismic sensor," *Arabian J. Geosci.*, vol. 12, no. 6, p. 179, 2019, doi: 10.1007/s12517-019-4368-2.
[21] M. Hehn, E. Sippel, and M. Vossiek, "An iterative extended Kalman filter for coherent measurements of incoherent network nodes in positioning systems," *IEEE Access*, vol. 8, pp. 36714–36727, 2020.
[22] R. Miesen, F. Kirsch, and M. Vossiek, "Holographic localization of passive UHF RFID transponders," in *Proc. IEEE Int. Conf. RFID*, Apr. 2011, pp. 32–37.
[23] M. Lipka, E. Sippel, and M. Vossiek, "An extended Kalman filter for direct, real-time, phase-based high precision indoor localization," *IEEE Access*, vol. 7, pp. 25288–25297, 2019.
[24] M. Vossiek and P. Gulden, "The switched injection-locked oscillator: A novel versatile concept for wireless transponder and localization systems," *IEEE Trans. Microw. Theory Techn.*, vol. 56, no. 4, pp. 859–866, Apr. 2008.
[25] M. Schtz, Y. Dobrev, C. Carlowitz, and M. Vossiek, "Wireless local positioning with SILO-based backscatter transponders for autonomous robot navigation," in *IEEE MTT-S Int. Microw. Symp. Dig.*, Apr. 2018, pp. 1–4.
[26] C.-C. Chen and H. Andrews, "Target-Motion-Induced radar imaging," *IEEE Trans. Aerosp. Electron. Syst.*, vol. AES-16, no. 1, pp. 2–14, Jan. 1980.
[27] Y. T. Chan and S. W. Rudnicki, "Bearings-only and Doppler-bearing tracking using instrumental variables," *IEEE Trans. Aerosp. Electron. Syst.*, vol. 28, no. 4, pp. 1076–1083, Oct. 1992.
[28] X. Li, C. Zhao, J. Yu, and W. Wei, "Underwater bearing-only and bearing-Doppler target tracking based on square root unscented Kalman filter," *Entropy*, vol. 21, no. 8, p. 740, 2019. [Online]. Available: https://www.ncbi.nlm.nih.gov/pmc/articles/PMC7515269/
[29] L. S. Cutler and C. L. Searle, "Some aspects of the theory and measurement of frequency fluctuations in frequency standards," *Proc. IEEE*, vol. 54, no. 2, pp. 136–154, Feb. 1966.
[30] E. Rubiola, *Phase Noise and Frequency Stability in Oscillators* (The Cambridge RF and Microwave Engineering Series). Cambridge, U.K.: Cambridge Univ. Press. [Online]. Available: https://www.cambridge.org/core/books/phase-noise-and-frequency-stability-in-oscillators/445C12C4ECBFCD7765116E61561EC0FE
[31] G. Zhai, H. Meng, and X. Wang, "A constant speed changing rate and constant turn rate model for maneuvering target tracking," *Sensors*, vol. 14, no. 3, p. 5239, 2014. [Online]. Available: https://www.ncbi.nlm.nih.gov/pmc/articles/PMC4003991/
[32] A. C. C. Olaya, C. E. Calosso, J.-M. Friedt, S. Micalizio, and E. Rubiola, "Phase noise and frequency stability of the Red-Pitaya internal PLL," *IEEE Trans. Ultrason., Ferroelectr., Freq. Control*, vol. 66, no. 2, pp. 412–416, Feb. 2019.
[33] G. S. Christiansen, "Modeling of PRML timing loop as a Kalman filter," in *Proc. IEEE GLOBECOM. Commun., Global Bridge*, vol. 2, Nov. 1994, pp. 1157–1161.
[34] I. Sharp and K. Yu, "Enhanced least-squares positioning algorithm for indoor positioning," *IEEE Trans. Mobile Comput.*, vol. 12, no. 8, pp. 1640–1650, Aug. 2013.
[35] B. M. Bell and F. W. Cathey, "The iterated Kalman filter update as a Gauss-Newton method," *IEEE Trans. Autom. Control*, vol. 38, no. 2, pp. 294–297, Feb. 1993.
[36] P. D. Teal, T. D. Abhayapala, and R. A. Kennedy, "Spatial correlation for general distributions of scatterers," *IEEE Signal Process. Lett.*, vol. 9, no. 10, pp. 305–308, Oct. 2002.
[37] C. Cahn, "Performance of digital phase-modulation communication systems," *IEEE Trans. Commun.*, vol. COM-7, no. 1, pp. 3–6, May 1959.
[38] P. S. Maybeck, *Stochastic Models, Estimation, and Control*. New York, NY, USA: Academic, Aug. 1982.
[39] Y. Bar-Shalom and X.-R. Li, *Estimation With Applications to Tracking and Navigation*. Hoboken, NJ, USA: Wiley, 2001.
[40] M. Smaoui-Kallel, Y. B. Jemaa, and M. Jaidane, "Adaptive PLL performances analysis for digital transmission context," in *Proc. 1st Int. Symp. Control, Commun. Signal Process.*, Mar. 2004, pp. 291–294.
[41] S. Thrun, W. Burgard, D. Fox, and R. C. Arkin, *Probabilistic Robotics*. Cambridge, MA, USA: MIT Press, Aug. 2005.
[42] P. Wright, "On minimum spanning trees and determinants," *Math. Mag.*, vol. 73, no. 1, pp. 21–28, Feb. 2000.
[43] L. Cao and H. M. Schwartz, "Exponential convergence of the Kalman filter based parameter estimation algorithm," *Int. J. Adapt. Control Signal Process.*, vol. 17, no. 10, pp. 763–783, Dec. 2003, doi: 10.1002/acs.774.
[44] R. L. Filler, "The acceleration sensitivity of quartz crystal oscillators: A review," *IEEE Trans. Ultrason., Ferroelectr., Freq. Control*, vol. 35, no. 3, pp. 297–305, May 1988.
[45] E. Sippel, M. Lipka, J. Geib, M. Hehn, and M. Vossiek, "*in-situ* calibration of antenna arrays within wireless locating systems," *IEEE Trans. Antennas Propag.*, vol. 68, no. 4, pp. 2832–2841, Apr. 2020.
[46] R. K. Mehra, "Approaches to adaptive filtering," *IEEE Trans. Autom. Control*, vol. AC-17, no. 5, pp. 693–698, Oct. 1972.
[47] T. K. Moon and W. C. Stirling, *Mathematical Methods and Algorithms for Signal Processing*. Upper Saddle River, NJ, USA: Prentice-Hall, 2000.

ERIK SIPPEL was born in Fürth, Germany, in 1991. He received the M.Sc. degree in electronic engineering from Friedrich-Alexander-Universität Erlangen-Nürnberg (FAU), Erlangen, Germany, in 2015, where he is currently pursuing the Ph.D. degree.

In 2016, he joined the Institute of Microwaves and Photonics, FAU. His current research interests include indoor localization, especially radar for near-field localization, antenna calibration, data transmission, and analog-to-digital conversion.

MARKUS HEHN (Graduate Student Member, IEEE) was born in Bamberg, Germany, in 1987. He received the M.Sc. degree in electrical engineering from Friedrich-Alexander-Universität Erlangen-Nürnberg (FAU), Erlangen, Germany, in 2016, where he is currently pursuing the Ph.D. degree.

In 2016, he joined the Institute of Microwaves and Photonics, FAU. His current research interests include radar for near-field localization and localization systems for indoor environment.

TOBIAS KOEGEL was born in Lauf, Germany, in 1995. He received the M.Sc. degree in electrical engineering from Friedrich-Alexander-Universität Erlangen-Nürnberg (FAU), Erlangen, Germany, in 2020, where he is currently pursuing the Ph.D. degree with the Institute of Microwaves and Photonics. His current research interests include radar and localization systems for indoor environments based on the UHR-RFID technology.

PATRICK GRÖSCHEL (Member, IEEE) was born in Nuremberg, Germany, in 1990. He received the M.Sc. degree in electronic engineering from Friedrich Alexander Universität (FAU), Erlangen, Germany, in 2016, where he is currently pursuing the Ph.D. degree. He joined the Institute of Microwaves and Photonics, FAU, in 2016. His research interests include the design and characterization of massive MIMO systems, error calibration and mitigation, communication and localization, and signal processing based on those systems.

ANDREAS HOFMANN was born in Bayreuth, Germany, in 1990. He received the M.Sc. degree in electrical engineering from Friedrich-Alexander-Universität Erlangen-Nürnberg (FAU), Erlangen, Germany, in 2016, where he is currently pursuing the Ph.D. degree with the Institute of Microwave and Photonics (LHFT). His current research interests include radars, transponders, and phase-locked-loops.

STEFAN BRÜCKNER was born in Kronach, Germany, in 1992. He received the M.Sc. degree in electronic engineering from Friedrich-Alexander-Universität Erlangen-Nürnberg (FAU), Erlangen, Germany, in 2019, where he is currently pursuing the Ph.D. degree. In 2019, he joined the Institute of Microwaves and Photonics, FAU. His current research interests include radar for close range applications, indoor positioning, Kalman filter for localization, and signal processing.

JOHANNA GEISS (Graduate Student Member, IEEE) was born in Lich, Germany, in 1992. She received the master's degree in electrical engineering from Friedrich-Alexander-Universität Erlangen-Nürnberg (FAU), Erlangen, Germany, in 2017, where she is currently pursuing the Ph.D. degree with the Institute of Microwaves and Photonics (LHFT). She is primarily working in the fields of radar-based localization, sensor-fusion, radar signal processing, radar calibration, and ego-motion estimation.

ROBERT SCHOBER received the Diploma (Univ.) and Ph.D. degrees in electrical engineering from Friedrich–Alexander University Erlangen–Nürnberg (FAU), Germany, in 1997 and 2000, respectively. From 2002 to 2011, he was a Professor and Canada Research Chair at The University of British Columbia (UBC), Vancouver, Canada. Since January 2012, he has been an Alexander von Humboldt Professor and the Chair for digital communication at FAU. His research interests include communication theory, wireless communications, and statistical signal processing. Since 2017, he has been listing as a Highly Cited Researcher by the Web of Science. He is a fellow of the Canadian Academy of Engineering and the Engineering Institute of Canada. He is a member of the German National Academy of Science and Engineering. He received several awards for his work, including the 2002 Heinz Maier-Leibnitz Award of the German Science Foundation (DFG), the 2004 Innovations Award of the Vodafone Foundation for Research in Mobile Communications, the 2006 UBC Killam Research Prize, the 2007 Wilhelm Friedrich Bessel Research Award of the Alexander von Humboldt Foundation, the 2008 Charles McDowell Award for Excellence in Research from UBC, the 2011 Alexander von Humboldt Professorship, the 2012 NSERC E. W. R. Stacie Fellowship, and the 2017 Wireless Communications Recognition Award by the IEEE Wireless Communications Technical Committee. From 2012 to 2015, he served as the Editor-in-Chief for the IEEE Transactions on Communications. He currently serves as a member for the Editorial Board of the Proceedings of the IEEE and a VP Publications for the IEEE Communications Society (ComSoc).

MARTIN VOSSIEK (Fellow, IEEE) received the Ph.D. degree from Ruhr-Universität Bochum, Bochum, Germany, in 1996. In 1996, he joined Siemens Corporate Technology, Munich, Germany, where he was the Head of the Microwave Systems Group, from 2000 to 2003. Since 2003, he has been a Full Professor with Clausthal University, Clausthal-Zellerfeld, Germany. Since 2011, he has been the Chair of the Institute of Microwaves and Photonics (LHFT), Friedrich-Alexander-Universität Erlangen-Nürnberg (FAU), Erlangen, Germany. He has authored or coauthored more than 300 articles. His research has led to over 90 granted patents. His current research interests include radar, transponder, RF identification, communication, and wireless locating systems. He is a member of the German National Academy of Science and Engineering (acatech) and the German Research Foundation (DFG) Review Board. He is a member of the German IEEE Microwave Theory and Techniques (MTT)/Antennas and Propagation (AP) Chapter Executive Board. He is a member of the IEEE MTT Technical Committees MTT-24 Microwave/mm-wave Radar, Sensing, and Array Systems, MTT-27 Connected and Autonomous Systems (as the Founding Chair), and MTT-29 Microwave Aerospace Systems. He has been a member of organizing committees and technical program committees for many international conferences. He has received more than ten best paper prices and several other awards. For example, he was awarded the 2019 Microwave Application Award from the IEEE MTT Society (MTT-S) for Pioneering Research in Wireless Local Positioning Systems. He is serving on the Advisory Board for the IEEE CRFID Technical Committee on Motion Capture and Localization. He has served on the review boards for numerous technical journals. From 2013 to 2019, he was an Associate Editor for the IEEE Transactions on Microwave Theory and Techniques.